Title

An Analysis of Isoclonal Antibody Formats Suggests a Role for Measuring PD-L1 with Low Molecular Weight PET Radiotracers

Journal

Molecular Imaging and Biology, 22(6)

ISSN

1536-1632

Authors

Wei, Junnian
Wang, Yung-hua
Lee, Chia Yin
et al.

Publication Date

2020-12-01

DOI

10.1007/s11307-020-01527-3

Peer reviewed

HHS Public Access

Author manuscript

Mol Imaging Biol. Author manuscript; available in PMC 2021 December 01.

Published in final edited form as:

Mol Imaging Biol. 2020 December ; 22(6): 1553–1561. doi:10.1007/s11307-020-01527-3.

An analysis of isoclonal antibody formats suggests a role for measuring PD-L1 with low molecular weight PET radiotracers

Junnian Wei[1,#], **Yung-hua Wang**[1,#], **Chia Yin Lee**[2], **Charles Truillet**[3], **David Y. Oh**[4,5], **Yichen Xu**[6], **Davide Ruggero**[5,6], **Robert R. Flavell**[1,5], **Henry F. VanBrocklin**[1,5], **Youngho Seo**[1,5], **Charles S. Craik**[5,7], **Lawrence Fong**[4,5], **Cheng-I Wang**[2], **Michael J. Evans**[1,5,7,*]

[1]Department of Radiology and Biomedical Imaging, University of California San Francisco 505 Parnassus Ave, San Francisco CA 94143

[2]Singapore Immunology Network, Agency for Science, Technology and Research (A*STAR), 8A Biomedical Grove Immunos #03-06, Biopolis Singapore 138648

[3]Imagerie Moleculaire In Vivo, INSERM, CEA, Univ. Paris Sud, CNRS, Universite Paris Saclay, CEA-Service Hospitalier Frederic Joliot, Orsay France, 94100

[4]Department of Medicine, University of California San Francisco, 513 Parnassus Ave, San Francisco CA 94143

[5]Helen Diller Family Comprehensive Cancer Center, University of California San Francisco, 505 Parnassus Ave, San Francisco CA 94143

[6]Department of Urology, University of California San Francisco, 505 Parnassus Ave, San Francisco CA 94143

[7]Department of Pharmaceutical Chemistry, University of California San Francisco, 505 Parnassus Ave, San Francisco CA 94143

Abstract

Purpose: The swell of new and diverse radiotracers to predict or monitor tumor response to cancer immunotherapies invites the opportunity for comparative studies to identify optimal platforms. To probe the significance of antibody format on image quality for PD-L1 imaging, we developed and studied the biodistribution of a library of antibodies based on the anti-PD-L1 IgG1 clone C4.

*To whom the correspondence should be addressed: Michael J. Evans, michael.evans@ucsf.edu.
#These authors contributed equally.

Conflict of Interest: The authors declare no conflicts of interest.

Ethical approval: All applicable international, national, and/or institutional guidelines for the care and use of animals were followed.

Ethical approval: This article does not contain any studies with human participants performed by any of the authors.

Procedure: A C4 minibody and scFv were cloned, expressed and characterized. The antibodies were functionalized with desferrioxamine and radiolabeled with Zr-89 to enable rigorous comparison to prior data collected using ^{89}Zr-labeled C4 IgG1. The biodistribution of the radiotracers was evaluated in C57Bl6/J or nu/nu mice bearing B16F10 or H1975 tumors, respectively, which are models that represent high and low tumor autonomous PD-L1 expression.

Results: The tumor uptake of the ^{89}Zr-C4 minibody was higher than ^{89}Zr-C4 scFv, and equivalent to previous data collected using ^{89}Zr-C4 IgG1. However, the peak tumor to normal tissue ratios were generally higher for ^{89}Zr-C4 scFv compared to ^{89}Zr-C4 minibody and ^{89}Zr-IgG1. Moreover, an exploratory study showed that the rapid clearance of ^{89}Zr-C4 scFv enabled detection of endogenous PD-L1 on a genetically engineered and orthotopic model of hepatocellular carcinoma.

Conclusion: In summary, these data support the use of low molecular weight constructs for PD-L1 imaging, especially for tumor types that manifest in abdominal organs that are obstructed by the clearance of high molecular weight radioligands.

Introduction:

Developing biomarkers to forecast which patients will be best served by cancer immunotherapies is a major unmet need for the oncology community [1]. As tissue biomarkers are fraught with false positivity and negativity for prediction of treatment response [2-3], the molecular imaging community has begun developing new technologies with the hope of overcoming these limitations [4].

Radiotracers for de novo predictions of tumor responses in treatment naive patients have primarily targeted T cell effector proteins for which there is a cognate therapeutic (e.g. CTLA4, PD-1, PD-L1) [5]. The rationale for imaging drug target concentration stems primarily from the following paradox: while protein expression is a prerequisite of tumor response, expression levels determined from immunohistochemistry of biopsied tumor tissue are not strongly predictive biomarkers[6]. One potential explanation is that intertumoral heterogeneity within a patient may create unintended sampling bias when studying the features of only a single biopsy. On this basis, the molecular imaging community has proposed that a more holistic measurement of target expression among all tumors in the patient with imaging could enable the development of better predictive metrics. Early imaging data from small patient cohorts suggest this could be true [7-9].

In the rush to keep pace with new drug discovery and clinical trials, the first human imaging studies have largely been conducted with radiolabeled therapeutic antibodies (e.g. ^{89}Zr-atezolizumab, ^{89}Zr-avelumab), as the ready access to GMP material accelerates the process of translation. However, it is not clear if bioactive immunoglobulins are optimal for imaging applications, and rigorous comparisons among the available repertoire of imaging probes are warranted to address this point. Indeed, earlier in the tracer development pipeline is a large and chemically diverse pool of radioligands that may have features better suited for imaging applications [5].

One open question germane to measuring immune checkpoint protein expression is whether there is an optimal antibody platform for imaging. While prior comparative studies show that small antibody platforms can produce images of a quality equivalent to IgGs within just a few hours, these studies were conducted with tumor antigens that are highly overexpressed (e.g. PSCA, CEA) [10]. Whether smaller antibody formats are broadly useful for a target like PD-L1 whose expression levels can vary significantly between patients (and likely also among tumors within patients) is an open question worthy of further investigation.

To address this question, we report herein a comparative analysis of antibody formats derived from the clone C4, an anti-PD-L1 antibody that we previously engineered and studied in the immunoglobulin format (~150 kDa) for nuclear imaging[11-12].

Materials and Methods:

General Methods:

B16 F10 and H1975 cells were acquired from ATCC and subcultured according to manufacturer's recommendations. Para-isothiocyanatobenzyl-DFO was obtained from Macrocyclics (Dallas, TX) and used without further purification. Zirconium-89 was purchased from 3D Imaging, LLC (Maumelle, AR).

Antibody cloning and expression:

The sequence of the scFv of clone C4 was arranged by connecting the VH to VL via a 15 amino acid (Gly4Ser)3 linker. The minibody was constructed by connecting the scFv to the CH3 domain of the human IgG1 via a 26 amino acids NSGAGTAAATHTCPPCGGGGSGGGGS linker. Both constructs carried a histidine tag at the C-terminus to facilitate purification and were cloned in the pTT5 vector. The proteins were expressed in HEK293 6E cells by transient transfection as described previously and purified using Qiagen's Ni-NTA agarose resin according to the manufacturer's instructions. A description of the bioconjugation as well as the radiochemistry protocol appears in the Supplemental Material.

Kd calculation:

Kinetic constants for the minibody and scFv antibody against human and mouse PD-L1 (Sino Biological Inc.) were determined via biolayer interferometry with an Octet RED384 instrument (ForteBio) using a previously described approach[11].

Animal studies:

Three to five week old male athymic nu/nu T cell deficient mice and immunocompetent male C57BL/6J mice were purchased from Charles River. Nu/nu mice were inoculated with 1.5 x 10^6 H1975 cells subcutaneously into one flank in a 1:1 mixture (v/v) of media (RPMI) and Matrigel (Corning). Tumors were palpable within 8-14 days after injection. C57BL/6J mice were inoculated with 1.5x 10^6 B16F10 subcutaneously into one flank in a 1:1 (v/v) mixture of Matrigel and DMEM. Tumors were palpable within 3-5 days after injection. The *Alb Cre; MYC^{Tg}; $KRAS^{G12D}$* mice were developed as previously reported [13]. The mice used in this study were female and approximately 1 year of age. The orthotopic model was

established by injection a single cloned mouse cell line derived from an *Alb Cre; MYC^{Tg}; $KRAS^{G12D}$* mouse tumor directly into the median lobe of the liver as previously reported [13]. Tumor outgrowth was confirmed by MRI within 10 days post implantation.

Small animal PET/CT:

Tumor bearing mice (n=4 per treatment arm) received ~200 μCi of radioconjugated antibody in 100 μL saline solution volume intravenously using a custom mouse tail vein catheter with a 28-gauge needle and a 100-150 mm long polyethylene microtubing. During the imaging procedure, animals were anesthetized with gas isoflurane at 2% concentration mixed with medical grade oxygen. The mice were imaged on a small animal PET/CT scanner (Inveon, Siemens Healthcare, Malvern, PA). Animals were scanned for 20 minutes for PET, followed by the CT acquisition for approximately 7 minutes.

The co-registration between PET and CT images was obtained using the rigid transformation matrix that was pre-calculated using a calibration procedure developed for this scanner since the geometry between PET and CT remained constant for each of PET/CT scans using the combined PET/CT scanner. A photon attenuation correction and scatter correction was performed for PET reconstruction using the co-registered CT-based attenuation map to ensure the quantitative accuracy of the reconstructed PET data.

Biodistribution studies:

Mice received between 40 and 300 μCi of radiotracer via tail vein injection for biodistribution studies. At a dedicated time point after radiotracer injection, animals were euthanized by cervical dislocation, and blood and tissues were removed, weighed and counted on a gamma-counter for accumulation of ^{89}Zr-radioactivity. The data were background-and decay-corrected and the tissue uptake was expressed in units of percentage injected dose per gram of dry tissue (%ID/g).

Digital autoradiography:

At a dedicated time point post injection of ^{89}Zr-C4 IgG1 or ^{89}Zr-C4 scFv, mice were anesthetized and were perfused with cold PBS via cardiac puncture. The tumor tissues were immediately collected and flash frozen in OCT on dry ice. Tissues were sectioned on a microtome at a thickness of 20 μm and immediately mounted on glass slides. The slides were then exposed on a GE phosphor storage screen, and the screen was developed on an Amersham Typhoon 9400 phosphorimager. H&E staining was performed by the Pathology core facility at UCSF. The autoradiography images were processed using ImageJ software.

Immunohistochemistry:

A section of the liver from the *Alb-Cre; MYC^{Tg}; $KRAS^{G12D}$* transgenic mouse model of hepatocellular carcinoma was subjected to antigen retrieval in Tris-EDTA buffer (10 mM Tris base, 1 mM EDTA solution, 0.05% Tween 20, pH 9.0) at 95° C for 15 min. After the antigen retrieval, the slide was blocked with IHC blocking buffer (eBioscience,San Diego, USA, catalog number: 00-4952-54) for 1 h. The slide was incubated in the PD-L1 primary antibody (1:200 dilution, Proteintech, Rosemont, USA, catalog number: 66248-1-Ig) for 1 h at room temperature, was washed with Tris buffered saline (TBS) 3 x 4 min. Then the slide

was incubated with a horseradish peroxidase (HRP) conjugated secondary antibody (1:500, Invitrogen, Carlsbad, USA, catalog number: A16072) for 45 min at room temperature. The slide was then washed with TBS 4 times, 4 min each time. The ImmPACT NovaRED HRP substrate (VECTOR LABORATORIES, Burlingame, USA, catalog number: SK-4805) was used for the staining and the hematoxylin was used for counterstain.

Statistical Analysis:

Data were analyzed using the unpaired, two-tailed Student's *t*-test using PRISM software. Differences at the 99% confidence level ($P < 0.01$) were considered to be statistically significant.

Results:

Synthesis and in vitro characterization of ^{89}Zr-C4 minibody and scFv.

The C4 minibody and scFv were cloned, expressed and purified using the protocol outlined in the Materials and Methods. The affinity of the minibody and scFv for the ectodomain of PD-L1 was calculated using biolayer interferometry, and the binding constants are summarized in Table 1. The minibody and scFv were conjugated to the chelator desferrioxamine B (DFO) by reacting commercial *p*-isothiocyanatobenzyl-DFO with solvent exposed ε-amino groups on lysine residues. We performed this coupling with the intent to measure biodistribution using Zr-89 as the radioisotope. Although shorter lived isotopes are generally preferred for studying smaller antibody platforms, we reasoned that maintaining consistent bioconjugaton and radiolabeling chemistry would be helpful to rigorously isolate the effects of antibody size on quantitative image features. Using biolayer interferometry, we confirmed that the DFO-antibody conjugates remained highly potent for PD-L1 (Table 1). The DFO-antibodies were radiolabeled via incubation with ^{89}Zr-oxalic acid for 120 min and purified using size exclusion chromatography. The radiochemical yield was consistently >95% and the radiochemical purity was >98%. The specific activity of either probe was approximately 6 μCi/μg, which was consistent with the specific activity we previously acquired for ^{89}Zr-C4 IgG1.

A comparison of the biodistribution of the C4 IgG1, minibody, and scFv in matched syngeneic mouse or human tumor models.

We first analyzed the biodistribution of the ^{89}Zr-minibody in mice. For this analysis, we chose to work with mice bearing B16 F10 (mouse melanoma) or H1975 (human non-small cell lung cancer) for two reasons. First, we have pre-existing biodistribution data showing specific binding of ^{89}Zr-C4 IgG in these models [11], Second, B16 F10 and H1975 model tumors with significantly different levels of PD-L1, and we previously calculate their respective B_{max} values to be ~ 90,000 fmol/mg and ~35,000 fmol/mg [11].

The biodistribution of the minibody was evaluated at 2, 8, 24, and 48 hours post injection in C57Bl6/J mice bearing a subcutaneous B16 F10 syngeneic tumors or nu/nu mice bearing a subcutaneous H1975 xenograft. Since we previously showed that C4 has negligible accumulation in PD-L1 null abdominal and thoracic tissues and does not cross the blood brain barrier, we focused our analysis on the radiotracer levels in standard reference tissues

(blood, muscle, bone), and major tissues related to clearance or host immunology (kidney, liver, spleen). Plotting the radiotracer uptake in the blood pool over time showed that the minibody had cleared by 24 hours post injection in either mouse background (Figure 1A, 1B and Table 2). Comparing the tumor uptake to the blood pool activity showed that, in both cases, tumor uptake significantly exceeded blood poll activity by 8 hours post injection. Tumor uptake also peaked at 24 hours post injection. The decline in tumor retention of the minibody tracer at 48 hours post injection is consistent with temporal pattern of tumor radiotracer uptake observed using ^{89}Zr-C4 IgG1 [11]. The overall biodistribution of radiotracer uptake among normal tissues in immunocompetent or athymic nu/nu mice was qualitatively similar (Figure 1C, 1D, and Table 2). Kidney associated activity was higher than liver at all time points, as has been previously reported for radiolabeled minibodies targeting unrelated proteins [14]. Tracer binding was observed in the spleen, consistent with the presence of PD-L1 expressing cells in this organ. Lastly, to confirm that tumor uptake requires intact antibody, we conducted a biodistribution study using ^{89}Zr-C4 minibody that was heat denatured (HD) prior to injection. The tumor associated activity of the cohort injected with HD radiotracer was significantly lower than the level observed with intact antibody at 24 hours post injection, as expected (Figure 1E).

We next evaluated the biodistribution of the ^{89}Zr-C4 scFv at 0.5, 1.5, and 2.5 hours post injection. In either animal model, the radiotracer rapidly cleared from the blood pool and was virtually undetectable at 2.5 hours post injection, as expected. Moreover, tumor uptake of the radiotracer exceeded blood pool and peaked at 1.5 hours post injection (Figure 2A, 2B, and Table 3). The level of radiotracer uptake was equal or lower in kidney, liver, spleen and bone compared to tumor at 1.5 hours post injection (Figure 2C and 2D).

After collecting these data, we calculated the tumor to normal tissue ratios to enable comparisons between biodistribution patterns among the antibody platforms (Table 4 and 5). We compared data at 72 hours post injection for the IgG1, 48 hours post injection for the minibody, and 2.5 hours post injection for the scFv, each of which represented the time points at which the peak tumor to blood ratio was observed (Figure 3A). At these time points, the minibody had a significantly higher tumor to blood ratio compared to the IgG1 or the scFv. The tumor to blood ratio for the scFv was significantly higher than the ratio for the IgG1. The minibody had a significantly lower tumor normal tissue ratio in liver, kidney and spleen compared to the scFv (and in some cases, the IgG1). The tumor to liver and tumor to spleen ratio for the scFv was significantly higher than the levels observed with the IgG1. Lastly, the tumor to muscle ratio for the IgG1 was significantly higher than the levels calculated for the minibody and the scFv (which were not significantly different).

It has been previously hypothesized that low molecular weight imaging probes can produce high quality images based in part on their ability to more freely diffuse through tumor tissue to access target protein compared to larger constructs like IgGs. On this basis, we next applied digital autoradiography to understand the relative distribution of the ^{89}Zr-scFv versus the ^{89}Zr-C4 IgG1 within a tumor. These data showed that the scFv was more evenly diffused throughout the tumor tissue compared to the IgG1, whose tumor uptake was more punctate and aligned with the exterior of the tumor (Figure 3B). Thus, the increased access of the scFv to interior regions of the tumor along with the tracer's rapid systemic clearance

may provide a mechanistic basis for the higher tumor to normal tissue ratios among well vascularized abdominal organs.

These data also suggested that ^{89}Zr-scFv PET might empower the measurement of PD-L1 expression on tumors within abdominal organs, especially those that might otherwise be obstructed on imaging with larger antibody formats. To test this hypothesis, we conducted an exploratory study evaluating the uptake of ^{89}Zr-C4 scFv in *Alb-Cre; MYC^{Tg}; KRAS^{G12D}* mice, a PD-L1 positive genetically engineered mouse model of hepatocellular carcinoma [13], A female mouse ~1 year of age was injected with ^{89}Zr-scFv, and we studied the localization of the tracer in liver tumors post mortem with autoradiography at 1.5 hours post injection. The tracer uptake was qualitatively higher in tumors compared to normal liver tissue and co-localized with PD-L1 expression determined using a discrete antibody clone and immunohistochemistry (Figure 4A and Supplemental Figure 1). To quantify the magnitude of radiotracer uptake in this tumor cells, we established a separate cohort of mice in which mouse cells derived from a PD-L1 positive *Alb-Cre; MYC^{Tg}; KRAS^{G12D}* tumor were implanted directly into the median lobe of the liver. This approach results in a primary tumor mass sufficiently large to microdissect, unlike the GEM mouse which develops small multifocal disease. A biodistribution study conducted at 1.5 hours post injection showed tumor uptake to be 1.92 ± 0.2% ID/g, commensurate with the levels observed in subcutaneous B16F10 tumors (Figure 4B).

Discussion:

In this report, we conduct the first isoclonal analysis of antibody formats to measure PD-L1 expression in the tumor microenvironment. A minibody and scFv version of anti-PD-L1 IgG1 we developed (termed C4) were cloned, expressed and characterized. The minibody and scFv were functionalized with desferrioxamine and radiolabeled with Zr-89 to enable rigorous comparison to prior data collected using ^{89}Zr-labeled C4 IgG1. Radiotracer biodistribution studies in two mouse tumor models with high or low PD-L1 expression revealed several insights. First, the tumor uptake of the ^{89}Zr-C4 minibody was higher than ^{89}Zr-C4 scFv in each tumor, and equivalent to levels observed with ^{89}Zr-C4 IgG1. Interestingly, the peak tumor to normal tissue ratios were generally higher for ^{89}Zr-C4 scFv in abdominal organs compared to ^{89}Zr-C4 minibody and ^{89}Zr-IgG1. These data led us to test whether ^{89}Zr-scFv enabled the detection of tumor autonomous PD-L1 expression on spontaneously arising or orthotopic hepatocellular carcinoma tumors. Autoradiography and biodistribution studies showed evidence of tumor detection. Collectively, these comparative data suggest for the first time a clear utility for studying PD-L1 expression with low molecular weight probes.

The tumor to blood ratios for the minibody between animal strains are generally comparable. The tumor to blood and tumor to muscle ratios for the scFv begin to diverge at 2.5 hours with higher levels observed in the nu/nu background. The %ID/g levels show that this is driven by persistent uptake in the H1975 tumor while the levels in B16F10 tumors begin to decline from 1.5 to 2.5 hours post injection. This phenomenon, namely a rise followed by a decline in tumor uptake of the radiotracer, was also observed over several days of imaging with ^{89}Zr-C4 IgG in C57Bl6/J mice with B16 F10 tumors. We have also reported

a similar pattern of biodistribution in this tumor type with ^{89}Zr-atezolizumab, although the decline was less dramatic compared to C4. These data suggest that factors beyond antigen expression levels are driving the %ID/g values at extended uptake times post injection, for example rate of antibody/receptor internalization and/or catabolism.

Other low molecular weight radiotracers targeting PD-L1 have previously been developed, including peptides and antibody fragments [15-17]. However, clearly demonstrating their merit has been challenging due to the lack of rigorous control studies to understand whether the lower absolute radiotracer uptake in tumors that accompanies probes with shorter biological half-lives is sufficiently offset by lower non-specific binding in normal tissues to result in overall better image quality. Moreover, the animal validation studies with small constructs to date have generally focused on subcutaneous tumor implants that derived from tumor types for which detection with a larger construct would not be challenging for common metastatic sites (e.g. breast cancer, non-small cell lung cancer). Our experimental design was intentionally responsive to these considerations, and our data now suggest that further developing low molecular weight constructs like ^{89}Zr-C4 scFv toward translation, or continuing to study in humans radiotracers like the adnectin ^{18}F-BMS986192 [9, 18], may glean more versatile radiotracers toward understanding the clinical utility of PD-L1 expression as a predictive biomarker.

We are optimistic these studies will motivate further comparative analyses among the vast array of experimental radiotracers to measure tumor immunology. The few comparative studies that predate our study are also quite revealing. For instance, analysis of the impact of size and glycosylation on the image quality of radiolabeled recombinant PD-1 variants found that aglycosylated, smaller protein constructs (~14 kDa) were superior for imaging PD-L1 expression [19]. Furthermore, our own work comparing the biodistribution of two equipotent anti-PD-L1 immunoglobulins (C4 and atezolizumab) showed remarkably different biodistributions in animal models, with C4 having a better tumor to normal tissue ratio, and atezolizumab preferentially accumulating in spleen over tumor [12]. These studies will hopefully motivate further comparisons toward nominating an optimal imaging platform well prior to conducting time and resource expensive human trials.

Supplementary Material

Refer to Web version on PubMed Central for supplementary material.

Acknowledgments

Funding: M.J.E. was supported by an American Cancer Society Research Scholar Grant (130635-RSG-17-005-01-CCE) and the National Institute Biomedical Imaging and Bioengineering (R01EB025207). L.F. was supported by a Prostate Cancer Foundation Challenge Grant and the National Cancer Institute (R01CA223484, U01CA233100, and U01CA244452). C.S.C. was supported by the National Cancer Institute (P41CA196276). D.R. was supported by the National Cancer Institute (R35CA242986). Small animal PET/CT studies were performed on the instrument supported by National Institutes of Health grant S10RR023051. Research from UCSF reported in this publication was supported in part by the National Cancer Institute of the National Institutes of Health under Award Number P30CA082103. The content is solely the responsibility of the authors and does not necessarily represent the official views of the National Institutes of Health. Research from Singapore Immunology Network in this publication was supported by the Category 3 Industrial Alignment Fund (IAF 311007) awarded by the Biomedical Research Council of A*STAR.

References

1. Schumacher TN, Kesmir C, van Buuren MM (2015) Biomarkers in cancer immunotherapy. Cancer Cell 27:12–14. [PubMed: 25584891]
2. Patel SP, Kurzrock R (2015) PD-L1 Expression as a Predictive Biomarker in Cancer Immunotherapy. Mol Cancer Ther 14:847–856. [PubMed: 25695955]
3. Havel JJ, Chowell D, Chan TA (2019) The evolving landscape of biomarkers for checkpoint inhibitor immunotherapy. Nat Rev Cancer 19:133–150. [PubMed: 30755690]
4. Ehlerding EB, England CG, McNeel DG, Cai W (2016) Molecular Imaging of Immunotherapy Targets in Cancer. J Nucl Med 57:1487–1492. [PubMed: 27469363]
5. Krekorian M, Fruhwirth GO, Srinivas M, et al. (2019) Imaging of T-cells and their responses during anti-cancer immunotherapy. Theranostics 9:7924–7947. [PubMed: 31656546]
6. Davis AA, Patel VG (2019) The role of PD-L1 expression as a predictive biomarker: an analysis of all US Food and Drug Administration (FDA) approvals of immune checkpoint inhibitors. J Immunother Cancer 7:278. [PubMed: 31655605]
7. Bensch F, van der Veen EL, Lub-de Hooge MN, et al. (2018) (89)Zr-atezolizumab imaging as a non-invasive approach to assess clinical response to PD-L1 blockade in cancer. Nat Med 24:1852–1858. [PubMed: 30478423]
8. Niemeijer AN, Leung D, Huisman MC, et al. (2018) Whole body PD-1 and PD-L1 positron emission tomography in patients with non-small-cell lung cancer. Nat Commun 9:4664. [PubMed: 30405135]
9. Huisman M, Niemeijer AL, Windhorst B, et al. (2020) Quantification of PD-L1 expression with [(18)F]BMS-986192 PET/CT in patients with advanced stage non-small-cell lung cancer. J Nucl Med.
10. Knowles SM, Wu AM (2012) Advances in immuno-positron emission tomography: antibodies for molecular imaging in oncology. J Clin Oncol 30:3884–3892. [PubMed: 22987087]
11. Truillet C, Oh HLJ, Yeo SP, et al. (2018) Imaging PD-L1 Expression with ImmunoPET. Bioconjug Chem 29:96–103. [PubMed: 29125731]
12. Moroz A, Lee CY, Wang YH, et al. (2018) A Preclinical Assessment of (89)Zr-atezolizumab Identifies a Requirement for Carrier Added Formulations Not Observed with (89)Zr-C4. Bioconjug Chem 29:3476–3482. [PubMed: 30227708]
13. Xu Y, Poggio M, Jin HY, et al. (2019) Translation control of the immune checkpoint in cancer and its therapeutic targeting. Nat Med 25:301–311. [PubMed: 30643286]
14. Hu S, Shively L, Raubitschek A, et al. (1996) Minibody: A novel engineered anti-carcinoembryonic antigen antibody fragment (single-chain Fv-CH3) which exhibits rapid, high-level targeting of xenografts. Cancer Res 56:3055–3061. [PubMed: 8674062]
15. De Silva RA, Kumar D, Lisok A, et al. (2018) Peptide-Based (68)Ga-PET Radiotracer for Imaging PD-L1 Expression in Cancer. Mol Pharm 15:3946–3952. [PubMed: 30037229]
16. Hu K, Kuan H, Hanyu M, et al. (2019) Developing native peptide-based radiotracers for PD-L1 PET imaging and improving imaging contrast by pegylation. Chem Commun (Camb) 55:4162–4165. [PubMed: 30810133]
17. Wissler HL, Ehlerding EB, Lyu Z, et al. (2019) Site-Specific Immuno-PET Tracer to Image PD-L1. Mol Pharm 16:2028–2036. [PubMed: 30875232]
18. Donnelly DJ, Smith RA, Morin P, et al. (2018) Synthesis and Biologic Evaluation of a Novel (18)F-Labeled Adnectin as a PET Radioligand for Imaging PD-L1 Expression. J Nucl Med 59:529–535. [PubMed: 29025984]
19. Mayer AT, Natarajan A, Gordon SR, et al. (2017) Practical Immuno-PET Radiotracer Design Considerations for Human Immune Checkpoint Imaging. J Nucl Med 58:538–546. [PubMed: 27980047]

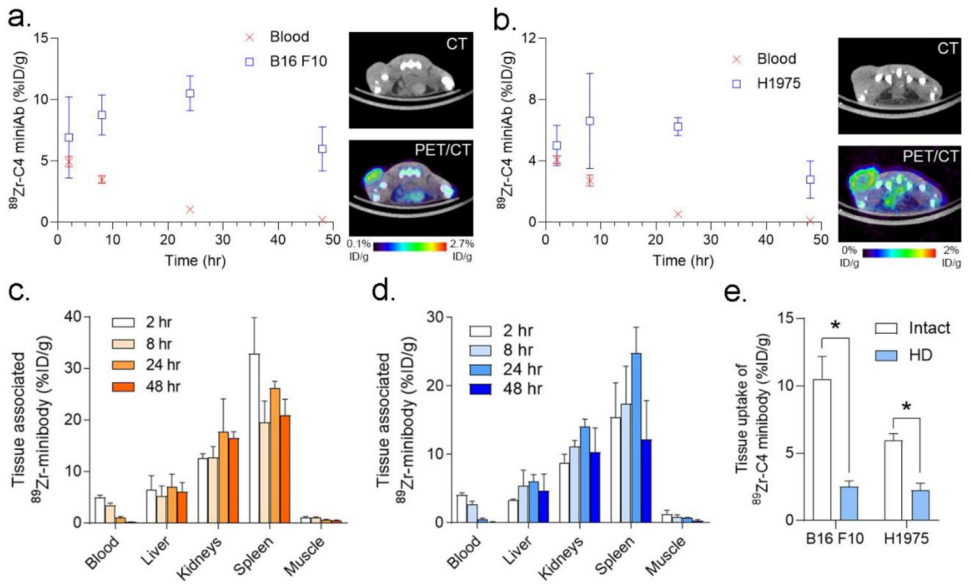

Figure 1. An analysis of the biodistribution of ^{89}Zr-C4 minibody over time in two animal models of cancer.

A. At left is shown a plot of the blood and tumor activity values for the radiolabeled C4 minibody at several time points after its injection into immunocompetent mice bearing B16F10 tumors. Tumor uptake was statistically higher than blood starting from 8 hours post injection. Tumor uptake peaked at 24 hours and declined from 24 to 48 hours, which mirrors the behavior we previously observed for ^{89}Zr-C4 IgG1 over a longer window of time. At right are shown transaxial CT and PET/CT taken at 24 hours post injection. The tumor is on the left hindlimb. **B.** At left is shown a plot of the blood and tumor activity values for the radiolabeled C4 minibody at several time points after its injection into nu/nu mice bearing H1975 xenografts. Tumor uptake was statistically higher than blood starting from 8 hours post injection. Tumor uptake peaked at 24 hours and declined from 24 to 48 hours. At right are shown transaxial CT and PET/CT taken at 24 hours post injection. The tumor is on the left hindlimb. C. Biodistribution data from select normal tissues from C57Bl6/J mice. **D.** Biodistribution data from select normal tissues from nu/nu mice. **E.** Biodistribution data showing that heat denaturing (HD) the radiolabeled ^{89}Zr-C4 minibody significantly reduces the tumor uptake compared to the intact antibody. The data were acquired at 24 hours post injection. *P < 0.01.

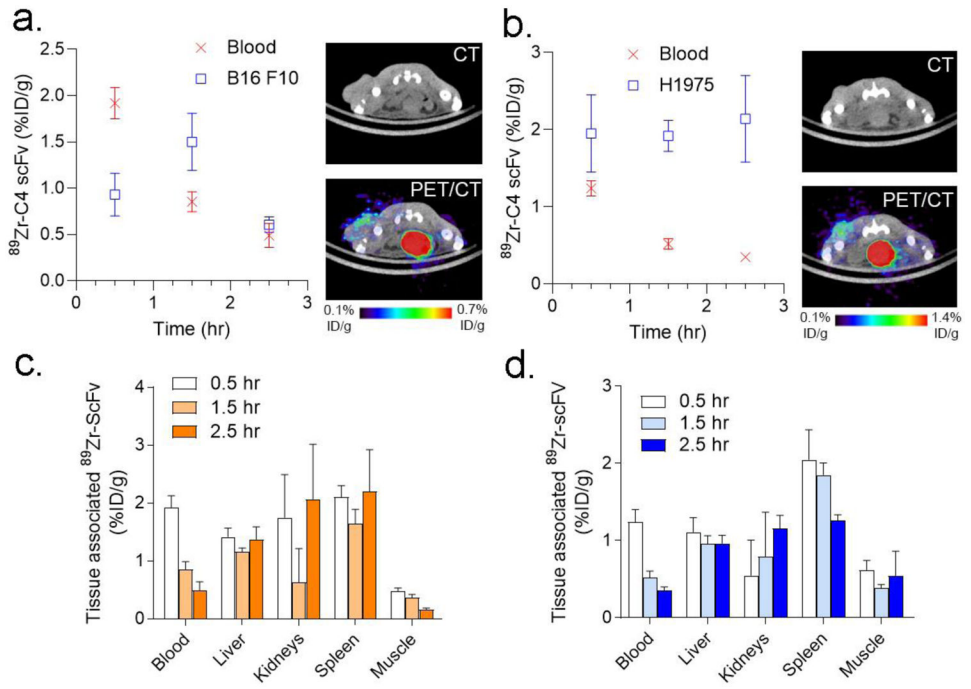

Figure 2. An analysis of the biodistribution of ^{89}Zr-C4 scFv over time in two animal models of cancer.

A. At left is shown a plot of the blood and tumor activity values for the radiolabeled C4 minibody at several time points after its injection into immunocompetent mice bearing implanted B16F10 tumor cells. Tumor uptake was statistically higher than blood starting from 1.5 hours post injection. Tumor uptake peaked at 1.5 hours and declined from 1.5 to 2.5 hours, which mirrors the behavior we observed with the ^{89}Zr-C4 minibody or IgG1 over a longer window of time. At right are shown transaxial CT and PET/CT taken at 1.5 hours post injection. The tumor is on the left hindlimb. **B.** At left is shown a plot of the blood and tumor activity values for the radiolabeled C4 scFv at several time points after its injection into nu/nu mice bearing H1975 xenografts. Tumor uptake was statistically higher than blood starting from 0.5 hours post injection. At right are shown transaxial CT and PET/CT taken at 1.5 hours post injection. The tumor is on the left hindlimb. C. Biodistribution data from select normal tissues from C57Bl6/J mice. **D.** Biodistribution data from select normal tissues from nu/nu mice.

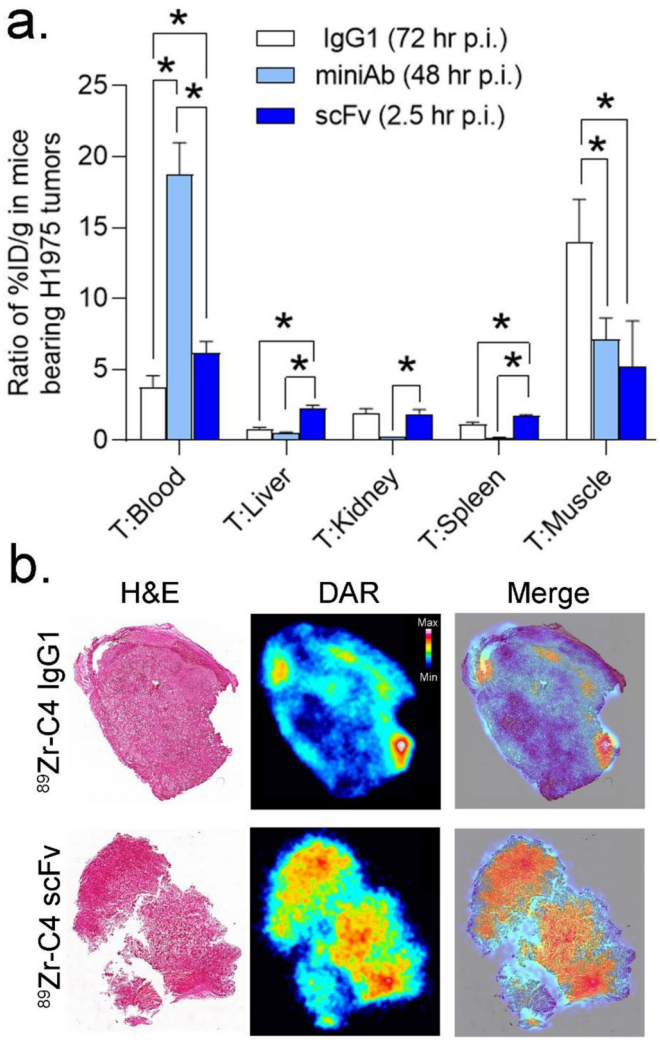

Figure 3. A comparison of the biodistribution of the IgG1, minibody, and scFv suggests a role for imaging with a low molecular weight platform.

A. A bar graph comparing the tumor to normal tissue ratios for the three antibody platforms. The time point post injection for comparison reflects the peak tumor to blood ratio for each platform. *P<0.01. B. Representative tumor sections show the distribution of the ^{89}Zr-C4 IgG1 and ^{89}Zr-C4 scFv using digital autoradiography (DAR). In general, the scFv more thoroughly diffused within tumor to access antigen. DAR was acquired from tumors after 72 hours of uptake time for the IgG1 and 1.5 hours of uptake time for the scFv.

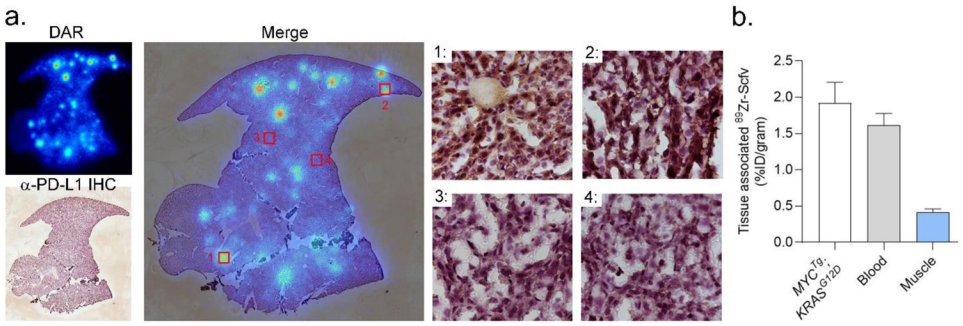

Figure 4. An exploratory imaging study suggests that ^{89}Zr-scFv may be useful for measuring PD-L1 expression levels on tumors within organs that would be obstructed by the clearance patterns of larger antibody formats.

A. DAR and anti-PDL1 immunohistochemistry (co-stained with hematoxylin) of a liver section from a 1 year old female *Alb Cre; MYC^{Tg}; KRAS^{G12D}* genetically engineered mouse model of heptacellular carcinoma. Multiple tracer avid foci are detected against the background of normal liver. At right are shown the merged images with the PDL1 immunohistochemistry magnified at 40X in selected fields of view to show the concordance between radiotracer binding and PD-L1 expression in tumor. Additional fields of view and tumor slices are shown in Supplemental Figure 1. **B.** Biodistribution data showing the uptake of ^{89}Zr-scFv in an orthotopic hepatocellular tumor established from a mouse cell line derived from the *Alb Cre; MYC^{Tg}; KRAS^{G12D}* GEM model.

Table 1:

A summary of the kinetic constants for the C4 minibody, scFv and their respective DFO-conjugates. The binding was assayed against the ectodomain of recombinant human PD-L1 using biolayer interferometry. The data are representative of two independent experiments. In the case of the K_D and the K_{dis} for the C4 minibody, the constants approached the limit of detection and the instrument was not capable of reporting error calculations.

Antibody	K_D (pM)	k_{on} (1/M*s)	K_{dis} (1/s)
C4 minibody	7.39	$2.61x10^5 \pm 2.2x10^3$	$1.93x10^{-6}$
C4 scFv	545 ± 51	$3.36x10^5 \pm 1.9x10^3$	$1.83x10^{-4} \pm 1.3x10^{-6}$
DFO-minibody	136 ± 9.5	$1.58x10^5 \pm 9.4x10^2$	$2.16x10^{-5} \pm 1.5x10^{-6}$
DFO-scFv	541 ± 5.1	$2.24x10^5 \pm 2.2x10^3$	$2.00x10^{-4} \pm 1.4x10^{-6}$

Table 2:

A summary of the biodistribution values for ^{89}Zr-C4 minibody in two mouse strains. The data are reported as mean ± standard deviation, n = 4 mice per time point.

Strain	nu/nu				C57Bl6/J			
Time (hr)	2	8	24	48	2	8	24	48
Blood	4.09±0.2	2.73±0.3	0.54±0.1	0.12±0.04	4.96±0.4	3.51±0.3	1.06±0.2	0.21±0.03
Liver	3.31±0.1	5.42±1.9	6.03±0.9	4.76±2.0	6.45±2.4	5.31±1.6	7.07±2.1	6.16±1.4
Kidney	8.82±1.0	11.17±0.7	14.07±0.9	10.37±3.0	12.58±0.7	12.77±1.8	17.7±5.5	16.55±1.0
Spleen	15.45±4.3	17.37±4.8	24.79±3.2	12.15±4.9	32.89±6.1	19.53±3.6	26.2±1.0	20.92±2.7
Muscle	1.27±0.5	0.86±0.2	0.70±0.07	0.33±0.1	1.14±0.1	1.08±0.1	0.7±0.07	0.48±0.1
Bone	5.57±0.4	5.86±0.5	4.77±0.2	4.19±0.9	4.51±1.1	4.15±0.8	4.63±0.3	2.70±1.1

Table 3:

A summary of the biodistribution values for ^{89}Zr-scFv in two mouse strains. The data are reported as mean ± standard deviation, n = 4 mice per time point.

Strain	**C57Bl6/J**			**nu/nu**		
Time (hr)	**0.5**	**1.5**	**2.5**	**0.5**	**1.5**	**2.5**
Blood	1.92±0.1	0.85±0.1	0.49±0.1	1.24±0.1	0.52±0.07	0.35±0.04
Liver	1.41±0.1	1.15±0.05	1.37±0.1	1.11±0.1	0.95±0.09	0.96±0.09
Kidneys	1.75±0.6	0.63±0.5	2.06±0.8	0.54±0.4	0.79±0.5	1.15±0.1
Spleen	2.10±0.1	1.64±0.2	2.199±0.62	2.04±0.3	1.85±0.1	1.25±0.06
Muscle	0.47±0.05	0.36±0.05	0.16±0.02	0.62±0.1	0.38±0.03	0.54±0.2
Bone	0.62±0.06	0.50±0.1	0.52±0.2	0.98±0.04	0.89±0.2	0.60±0.04

Table 4:

Tumor to normal ratios over time for the ^{89}Zr-minibody in two mouse backgrounds.

Strain	**C57Bl6/J**				**nu/nu**			
Time (hr)	**2**	**8**	**24**	**48**	**2**	**8**	**24**	**48**
Blood	1.40±0.1	2.52±0.2	10.14±2.0	28.44±4.5	1.23±0.08	2.47±0.3	12.16±3.0	18.79±2.2
Liver	1.25±0.5	1.84±0.7	1.69±0.8	1.04±0.3	1.51±0.07	1.36±0.4	1.05±0.1	0.79±0.5
Kidneys	0.55±0.04	0.70±0.1	0.64±0.2	0.36±0.02	0.57±0.07	0.59±0.04	0.44±0.03	0.31±0.1
Spleen	0.21±0.04	0.46±0.09	0.40±0.01	0.29±0.03	0.35±0.1	0.41±0.1	0.25±0.03	0.29±0.2
Muscle	6.14±0.7	8.17±1.1	15.15±2.0	13.55±4.4	4.45±1.4	8.68±3.7	8.97±1.1	11.89±9.5
Bone	1.25±0.1	1.51±0.1	2.21±0.1	1.51±0.4	1.22±0.5	1.68±0.4	1.35±0.09	1.45±1.2

Table 5:

Tumor to normal ratios over time for the ^{89}Zr-scFv in two mouse backgrounds.

Strain	**nu/nu**			**C57Bl6/J**		
Time (hr)	**0.5**	**1.5**	**2.5**	**0.5**	**1.5**	**2.5**
Blood	1.59±0.1	3.76±0.7	6.16±0.2	0.48±0.04	1.79±0.2	1.31±0.3
Liver	1.76±0.3	2.03±0.2	2.24±0.2	0.66±0.06	1.30±0.07	0.45±0.07
Kidneys	7.49±6.4	4.61±4.37	1.88±0.2	0.66±0.43	4.28±3.1	0.39±0.3
Spleen	0.97±0.1	1.04±0.09	1.71±0.1	0.44±0.04	0.93±0.1	0.31±0.1
Muscle	3.24±0.6	5.05±0.6	5.22±3.2	1.98±0.2	4.21±0.7	3.84±0.7
Bone	1.51±0.1	3.44±1.65	1.54±1.1	1.99±0.1	2.25±0.5	3.57±0.3